Journal of Solid State Chemistry 183 (2010) 1652–1662

Contents lists available at ScienceDirect

Journal of Solid State Chemistry

journal homepage: www.elsevier.com/locate/jssc

Structural and dielectric/ferroelectric properties of $(La_{1-x}Nd_x)_2Ti_2O_7$ synthesized by sol–gel route

Zhenmian Shao [a,b,c,d], Sébastien Saitzek [a,b,c,*], Pascal Roussel [a,c,d], Olivier Mentré [a,c,d], Felicia Prihor Gheorghiu [e], Liliana Mitoseriu [e], Rachel Desfeux [a,b,c]

[a] Univ Lille Nord de France, F-59000 Lille, France
[b] UArtois, UCCS, F-62300 Lens, France
[c] CNRS, UMR 8181, F-59650 Villeneuve d'Ascq, France
[d] ENSCL, UCCS, F-59652 Villeneuve d'Ascq, France
[e] University Al. I. Cuza Iasi, Department of Physics, Bv. Carol I, 11, Iasi 700506, Romania

ARTICLE INFO

Article history:
Received 1 March 2010
Received in revised form
29 April 2010
Accepted 4 May 2010
Available online 12 May 2010

Keywords:
$La_2Ti_2O_7$
$Nd_2Ti_2O_7$
Perovskite layered structure
Sol–gel
X-ray diffraction
Dielectric properties

ABSTRACT

A series of compounds with the general formula $(La_{1-x}Nd_x)_2Ti_2O_7$ ($0.0 \le x \le 1.0$) has been prepared by the sol–gel method. The decomposition of the gel was characterized by thermo-gravimetric analysis coupled to mass spectrometry, indicating the reaction is achieved above 850 °C. The lattice parameters versus x show an expected decrease in the a and b parameters while c and the β angle remain almost unchanged with respect to the monoclinic symmetry conserved for the full solid solution. Dielectric, piezoelectric and ferroelectric properties were measured on the entire series.

© 2010 Elsevier Inc. All rights reserved.

1. Introduction

Lanthanide titanium oxides with the general formula $Ln_2Ti_2O_7$ (Ln=lanthanides) have been considerably studied these last years due to their particular interests. Indeed, these compounds show a number of attractive properties, and we can cite among other: photocatalysis for water splitting [1–3]; a great ability for the realization of immobilization matrices of highly active radio-nuclides from nuclear wastes [4]; photo-luminescent properties when doped with rare earth ions [5–6]; ferroelectric [7,8] and piezoelectric [9] properties mainly used for the elaboration of high temperature devices.

$Ln_2Ti_2O_7$ compounds adopt a perovskite layered structure for Ln=La to Nd [1,7], while they prefer a pyrochlore type for Ln=Sm to Lu, [1,10,11]. The stability of these structures depends on the ratio between the cations radii of Ln^{3+} and Ti^{4+}. For $r(Ln^{3+})/r(Ti^{4+})$ included in the range {1.46–1.78}, the formed compound will adopt a pyrochlore-like structure. For ratio higher than 1.78, the layered perovskite type is preferred. Finally for ratio lower than 1.46, the formed compound will favor a defect fluorite structure [12]. Thus, $La_2Ti_2O_7$ (hereafter LTO) and $Nd_2Ti_2O_7$ (hereafter NTO) compounds, concerned in this work, crystallize in a perovskite layered structure according to the ratios: $r(Ln^{3+})/r(Ti^{4+})$=1.92 and 1.83, respectively, using ionic radii from Shannon [13].

$La_2Ti_2O_7$ was reported to be a ferroelectric material with a high Curie temperature (T_C=1500 °C). It has a dielectric constant in the range ε_r=42–62, with a low-temperature coefficient as well as a low dielectric loss at microwave frequency [14]. LTO crystallizes in a monoclinic structure with the $P2_1$ space group: a=7.8114(2) Å, b=5.5474(1) Å, c=13.0185(1) Å, β=98°43′(1), Z=4, and ρ=5.78 g/cm^3 [15]. Ferroelectric properties of $La_2Ti_2O_7$ single-crystal are characterised by a low spontaneous polarization: P_s=5 μC/cm^2 and a coercive field: E_c=45 kV/cm, with the polarization oriented along the b-axis (polar axis) [15].

Among various $Ln_2Ti_2O_7$ compounds with a layered perovskite structure, LTO is the most studied mainly for its dielectric properties. Ishizawa et al. [16] have shown that the structure changes from monoclinic ($P2_1$) to orthorhombic phase ($Cmc2_1$) at temperatures higher than 780 °C. Above 1500 °C, the structure undergoes further transformation into the paraelectric phase (Cmcm) [16]. Schmalle et al. [17] showed that $La_2Ti_2O_7$ crystals are systematically twinned, the twinning operation being a mirror

* Corresponding author at: Université d'Artois, Unité de Catalyse et de Chimie du Solide, UCCS, Équipe Chimie du Solide, CNRS-UMR 8181, Faculté des Sciences Jean Perrin, F-62300 LENS, France. Fax: +33 321177955.
E-mail address: sebastien.saitzek@univ-artois.fr (S. Saitzek).

0022-4596/$ - see front matter © 2010 Elsevier Inc. All rights reserved.
doi:10.1016/j.jssc.2010.05.004

plane perpendicular to the c^*-axis affecting only the oxygen positions in the structure. The angle between a^*_{twinI} and a^*_{twinII} is 17.12°.

NTO is isostructural with $La_2Ti_2O_7$, monoclinic, space group $P2_1$, $a=7.68(2)$ Å, $b=5.48(2)$ Å, $c=13.02(3)$ Å, $\beta=98°28'(5)$, $Z=4$, and $\rho=6.08$ g/cm^3 [18]. $Nd_2Ti_2O_7$ single crystals were found to be ferroelectric with a weak spontaneous polarization P_s of 9 μC/cm^2 and a high coercive field $E_c=200$ kV/cm at room temperature [18].

Among numerous routes for preparing polycrystalline $Ln_2Ti_2O_7$ (Ln=La or Nd) phases, such as standard high temperature solid-state reaction [19], polymerized complex method [20,21], hydrothermal synthesis [22], metallorganic decomposition method [23] and sol–gel synthesis [24,25], we selected the latter in order to reach $(La_{1-x}Nd_x)_2Ti_2O_7$ compounds ($0 \le x \le 1$).

The substitution of La^{3+} for Nd^{3+} in LTO compounds has been investigated in several fields, e.g. ferroelectric devices [9,26], photocatalysts [27], magnetoelectric emission [28], phosphors when doped with rare earth [29], and high temperature dielectric or piezoelectric devices [30,31]. In these studies, the reported substitution ratio of La^{3+} for Nd^{3+} is 0.4–0.6%, 10% or 50%. However, to the best of our knowledge, the existence of $(La_{1-x}Nd_x)_2Ti_2O_7$ complete solid solution has never been mentioned yet. Sayir et al. [9] reported electrical measurement on Nd-doped $La_2Ti_2O_7$ powders. At least, the effect of the Nd substitution is announced to increase the polarization while no structural features have been reported. The objective of this paper is to characterize the structural and dielectric/ferroelectric properties of the $(La_{1-x}Nd_x)_2Ti_2O_7$ solid solution. According to the selected sol–gel method, the gel decomposition stage has been characterized by thermal analysis. Our XRD characterization has been completed by a microstructural analysis using scanning electron microscopy (SEM). Finally, dielectric, piezoelectric and ferroelectric measurements carried out on densified $(La_{1-x}Nd_x)_2Ti_2O_7$ ceramic pellets, cooled in air or O_2, show interesting properties assorted with rather low dielectric losses.

2. Experimental

$(La_{1-x}Nd_x)_2Ti_2O_7$ powders have been synthesized using the sol–gel method previously described in [32]. The starting precursors are $La(NO_3)_3 \cdot 6H_2O$ (99.99%, Sigma Aldrich), $Nd(NO_3)_3 \cdot 6H_2O$ (99.9%, Alfa Aesar) and titanium isopropoxide ($Ti[OCH(CH_3)_2]_4$ (98.0%, Acros Organics). A first solution is obtained by mixing two solvents, 2,4-pentadione ($CH_3COCH_2COCH_3$, 99+%, Sigma Aldrich) and 2-methoxyethanol ($HO(CH_2)_2OCH_3$, 99.0%, Sigma Aldrich), then adding the titanium precursor. Separately, a second solution is achieved by mixing neodymium and lanthanum nitrates in 2-methoxyethanol solvent at approximately 50 °C. The molar ratio La/Nd is adjusted to meet the final stoichiometry of the solid solution. Finally, the two solutions previously described are mixed, with continuous stirring at 50 °C. The process is schematized in Fig. 1. The molar ratio of La+Nd precursors/$Ti(OPr^i)_4$/2,4-pentadione/2-methoxyethanol is 1/1/1.5/25.5.

The gels were dried from 100 to 300 °C for 3 h, and then calcined at 700 °C for 6 h and then at 1100 °C for 12 h after an intermediate grinding. Depending on x, the color of the sample changes from white to purple pastel. Note also that, starting from similar gels, we have recently shown the possibility to deposit oriented films by the spin-coating technique [32]. For the electric measurements, 10 mm diameter pellets were pressed at 0.2 MPa in a Perkin-Elmer Hydraulishe Presse and sintered at 1250 °C for 24 h.

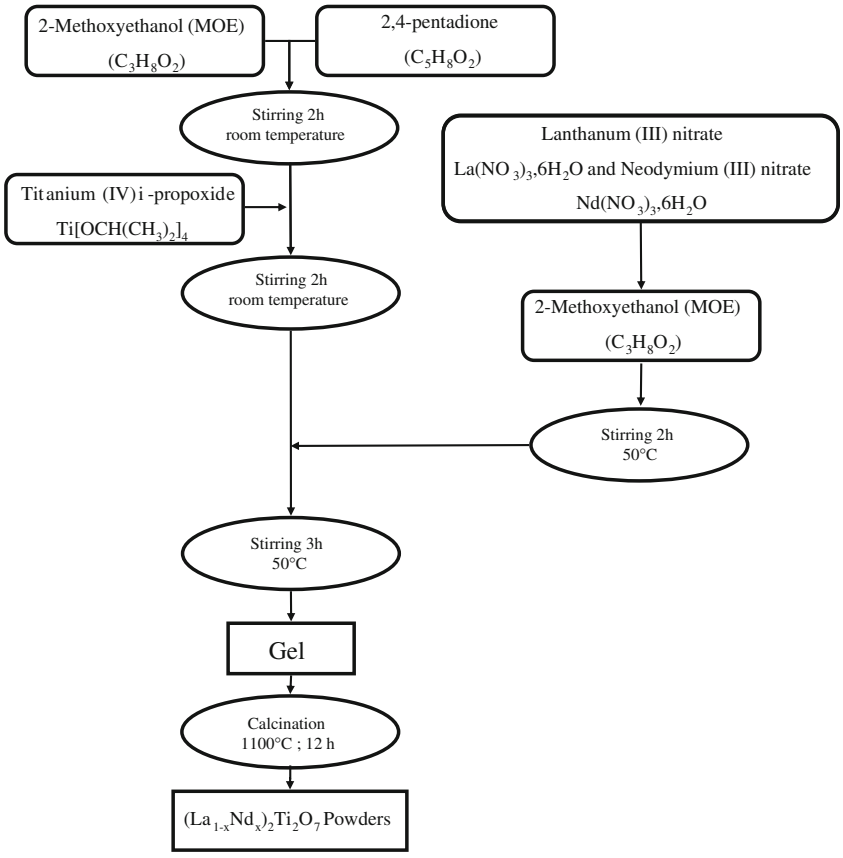

Fig. 1. Flowchart of the sol–gel route.

Thermal analyses have been performed using a TG-DTA-SETARAM 92-1600 system coupled with a Mass Spectrometer PFEIFFER-Omnistar GSD 3010; the sweep rates are 5 °C/min in air.

XRD patterns were collected on a Huber G670 diffractometer in a Guinier asymmetric transmission setup (λ-Cu-$K\alpha$1). The lattice parameters have been least-squares refined using the Unit Cell program [33]. The XRD patterns of pellets have been recorded in the range 2θ=[10–60°] on a D8 Bruker diffractometer in a Bragg–Brentano setup, also equipped with copper X-ray source. The grain morphology and the average grain size were observed by SEM using a FEG Hitachi 5-4700 microscope.

For the electrical measurements, sintered samples were cut in parallel-plate pieces and gold electrodes were deposited by *rf*-sputtering on the polished surfaces. The complex impedance was determined in the frequency domain 20 Hz–2 MHz at room temperature using an impedance bridge type Agilent E4980A Precision LCR Meter and in the range 1 MHz–1 GHz with an impedance analyzer type Agilent E4991A RF. The dielectric holder

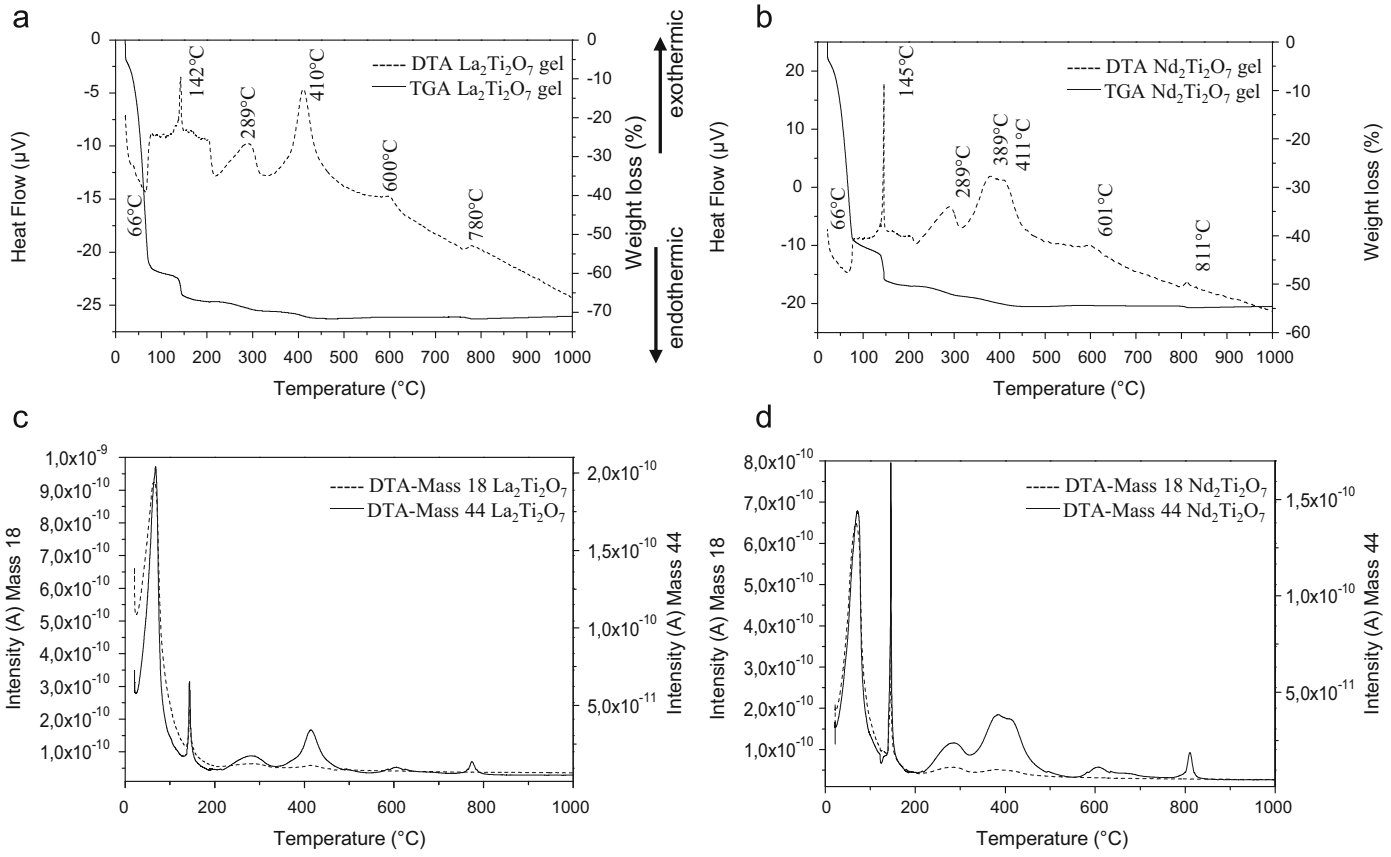

Fig. 2. Thermo-gravimetric and differential thermal analysis (TG-DTA) plot coupled with mass spectrometry (MS) analysis: (a) TG-DTA of $La_2Ti_2O_7$ gels; (b) TG-DTA of $Nd_2Ti_2O_7$ gels; (c) TG-TDA-MS 18 (H_2O) and 44 (CO_2) of $La_2Ti_2O_7$ and (d) TG-DTA-MS 18 (H_2O) and 44 (CO_2) of $Nd_2Ti_2O_7$.

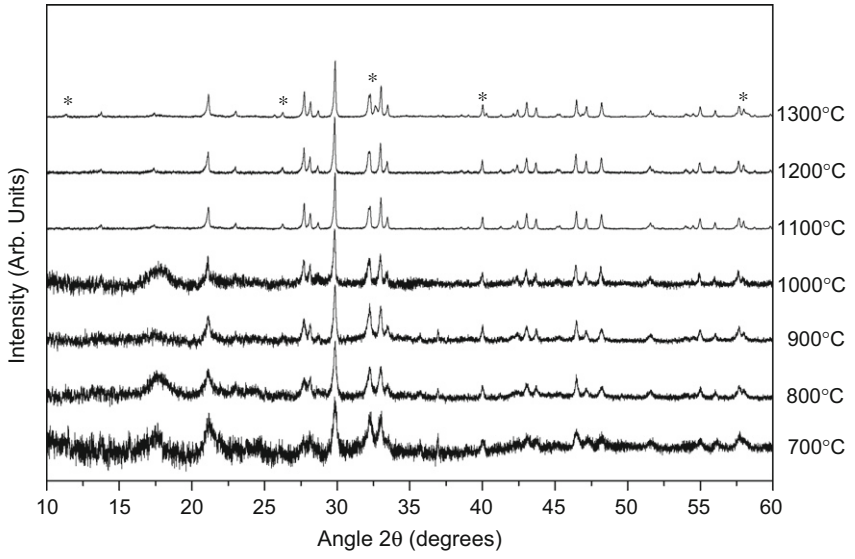

Fig. 3. XRD patterns of products obtained by various calcination temperatures for the $La_2Ti_2O_7$ gel precursor. *Peaks attributed to $La_2Ti_3O_9$ (JCPDS no. 26-0827).

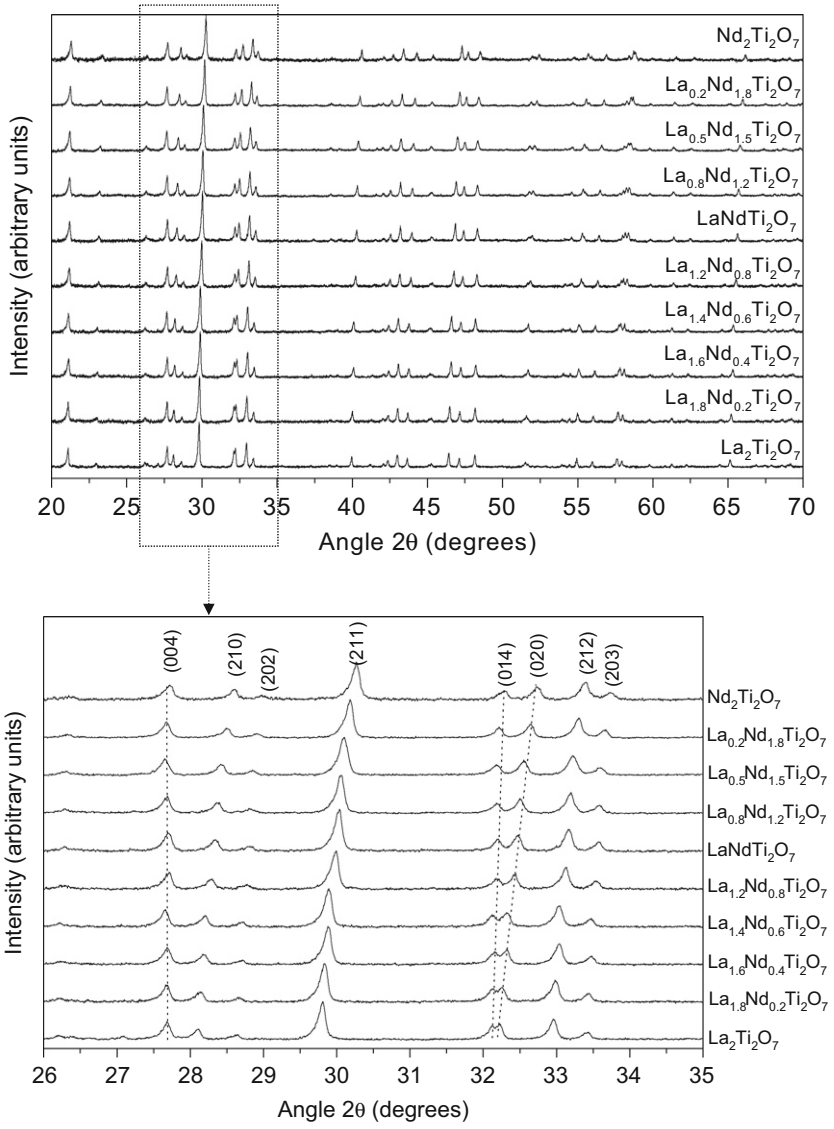

Fig. 4. XRD patterns of $(La_{1-x}Nd_x)_2Ti_2O_7$ powders for various x values. The (hkl) peaks positions (with h and $k \neq 0$) change with x values while the (00l) peaks positions remain unaffected.

allowed to apply a one-directional stress to the sample (high/low options), in order to qualitatively check the possible piezoelectricity of the ceramic samples. The $P(E)$ loops at room temperature were recorded under a sinusoidal waveform of amplitudes $E_0 = 0.5$ MV/m by using a modified Sawyer–Tower circuit in which the high voltage was obtained from a function generator coupled with a TREK 30/20A-H-CE amplifier. Polarization loops were recorded by placing the ceramic pellets in a cell containing transformer oil.

3. Results and discussion

3.1. Thermal analysis

We carried out thermo-gravimetric analysis (TGA) and differential thermal analysis (DTA) on the gels to determine the optimal calcinations temperature. TGA and DTA plots of LTO and NTO precursors are shown in Fig. 2. As expected, a similarity in the decomposition process is observed for both compounds. An endothermic peak in DTA and a fast weight loss appear at around 80 °C. It corresponds to the water loss (mass 18) out of the gel, as shown from mass spectrometry (Fig. 2c and d). The release of 2-methoxyethanol solvent is also observed at this temperature.

Secondly, a sharp exothermic peak is visible around 140 °C. This peak is likely to be due to the evaporation of the 2,4-pentadione, which has a boiling point of 139 °C. The mass spectrometer measurement realised on 28 and 44 mass (for CO and CO_2, respectively) shows a clear departure from carbonaceous material. Then, three broad exothermic peaks centered at 280–300, 370–420 and 590–610 °C are attributed to the combustion of organic groups of the precursor (these combustions accompanied by low mass loss). For $La_2Ti_2O_7$ and $Nd_2Ti_2O_7$, the mass 44 spectrometry confirms this assumption (Fig. 2c and d).

Finally, a little exothermic peak at 780 °C for $La_2Ti_2O_7$ or 811 °C for $Nd_2Ti_2O_7$ is observed. To explain this peak, two assumptions can be made. In a first hypothesis, it can be explained by the monoclinic/orthorhombic phase transition described by Ishizawa et al. [16] for LTO at 780 °C. A second hypothesis is that it corresponds to a weak loss of carbonaceous material during the stage of crystallization even at such a high temperature. The first hypothesis appears to be an easy shortcut, but it should lead to an endothermic peak as described by Zhao et al. [23], and can thus be ruled out. In addition, a DTA study conducted on final powders of

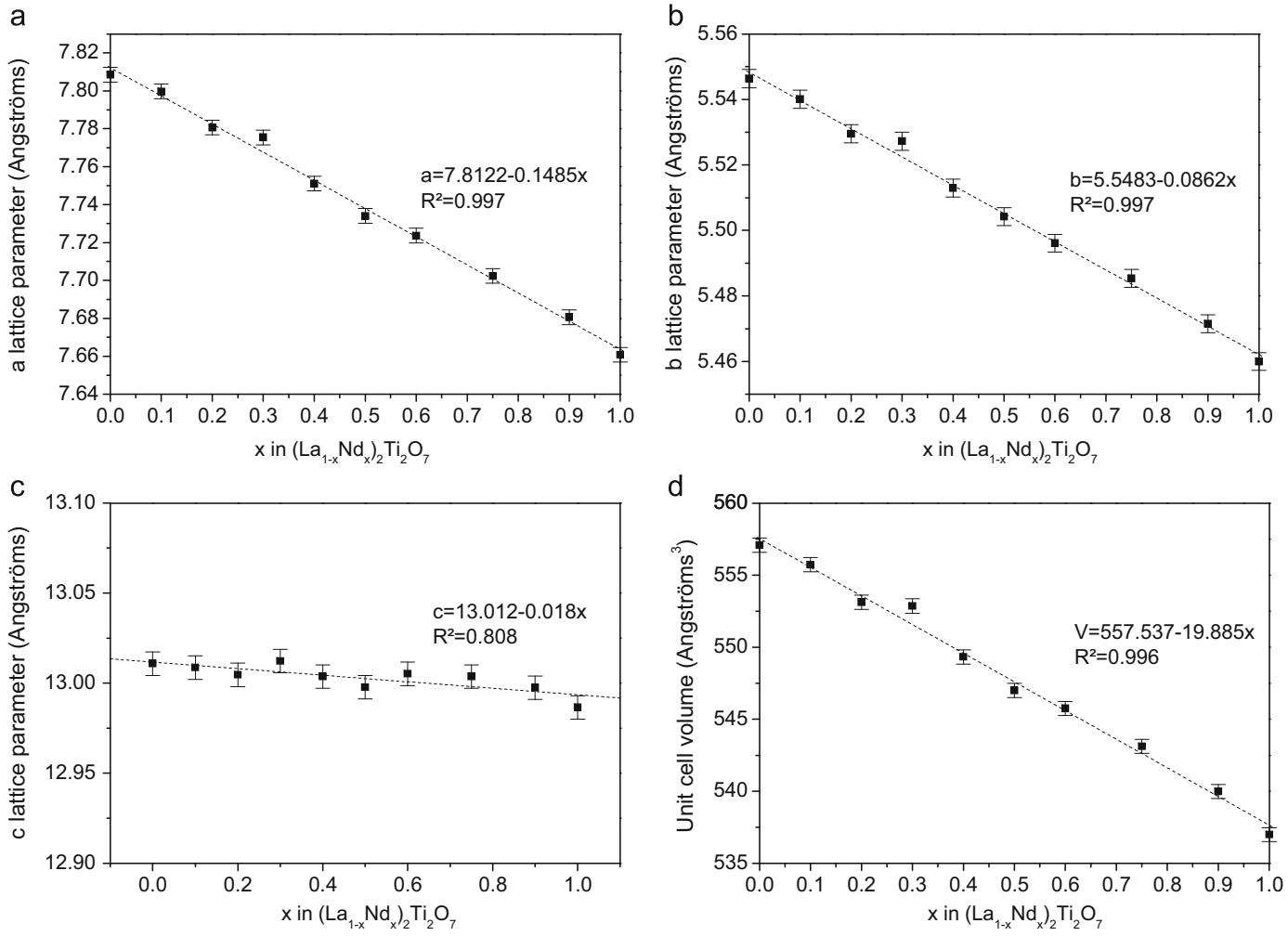

Fig. 5. The variation of $(La_{1-x}Nd_x)_2Ti_2O_7$ unit cell parameters versus x values.

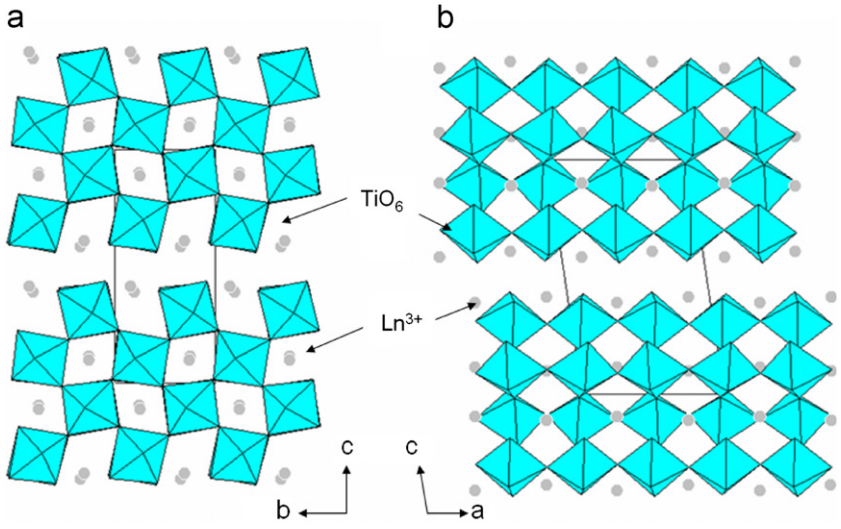

Fig. 6. The crystal structure of monoclinic $Ln_2Ti_2O_7$ showing slabs of corner-sharing TiO_6 octahedra.

LTO and NTO did not show any peak at these temperatures. Indeed, Fig. 2c and d clearly shows the departure of CO_2, which is perfectly coherent with the remaining organic parts. At this temperature, the latest carbon constituents leave the amorphous structure and the compound crystallizes (which will be later confirmed by the XRD analysis, see next section).

XRD patterns of $La_2Ti_2O_7$ prepared by the sol–gel route under different temperatures are shown in Fig. 3. This step was

undertaken to optimize the synthesis of undoped LTO. It starts to form above 700 °C. XRD peaks gradually increase until 1000 °C. From 1000 to 1100 °C, the intensity changes are drastic. The full-width at half-maximum (FWHM) of the lines becomes more narrow, such that a final firing at 1100 °C was chosen to optimize the crystallinity. Note that at 1300 °C, a second phase attributed to $La_2Ti_3O_9$ (JCPDS no. 26-0827) appears. This phase is a defected perovskite, which could increase the electric conductivity [9].

3.2. Structural characterizations and morphology

XRD patterns of $(La_{1-x}Nd_x)_2Ti_2O_7$ $(0 \le x \le 1)$ are shown in Fig. 4. The two end-members display the typical XRD patterns, i.e. LTO: JCPDS 81-1066; NTO: JCPDS 33-0942. The full solid solution adopts the monoclinic structure with $P2_1$ space group. The inset of Fig. 4 pictures an anisotropic evolution of the lattice parameters against x, as deduced from the different XRD lines depending on hkl values. Thus, a and b parameters decrease with increasing values of x from 7.80 to 7.66 and 5.54–5.46 Å, respectively, while the c parameter remains almost constant. Consequently, volume cell follows the a and c decrease versus x behavior. The evolutions of the lattice parameters versus x (Fig. 5) follow a Vegard's law [34], at least in agreement with the existence of the full La/Nd solid solution.

The structure of $Ln_2Ti_2O_7$ consists of distorted perovskite-like blocks (with four corner-sharing TiO_6 octahedra along their thickness) separated by double layers of Ln cations. Along the $\vec{a}$ and $\vec{b}$ axis, these compounds present infinite corner-sharing planes of TiO_6 octahedra, however interrupted every four octahedra along the $\vec{c}$ axis. So, the variation of the cationic size ($La^{3+}=1.160$ Å, $Nd^{3+}=1.109$ Å) inside the perovskite cage should influence significantly the a and b cell parameters according to the dimensionality along these axes. On the contrary, following the $\vec{c}$ axis, the less dense Ln-interleaves would behave as compressible media to counterbalance the (a, b) evolution. Thus, the modification of the La/Nd ratio does not affect significantly the value of c (Fig. 6).

To observe a possible evolution of the crystal morphology versus the substitution rate, we recorded SEM images for powders with $x=0$, 0.5 and 1. These are shown in Fig. 7. There is no significant change of the grain shape depending on the composition. Similar morphologies with characteristic dimension ~ 1 μm for grains have already been observed on $La_2Ti_2O_7$ and $Nd_2Ti_2O_7$ powders elaborated by solid way at 1100 °C during 300 h [35,36]. In the present study, the average size was determined by a statistical study performed on a hundred grains and several SEM images. We can notice that the values of average size and dispersion decrease with increase in the Nd content: 0.70 ± 0.20, 0.60 ± 0.15 and 0.40 ± 0.10 μm for $La_2Ti_2O_7$, $LaNdTi_2O_7$ and $Nd_2Ti_2O_7$, respectively. Note that no heterogeneity in the chemical analysis was evidenced by energy dispersive spectrometry (EDS).

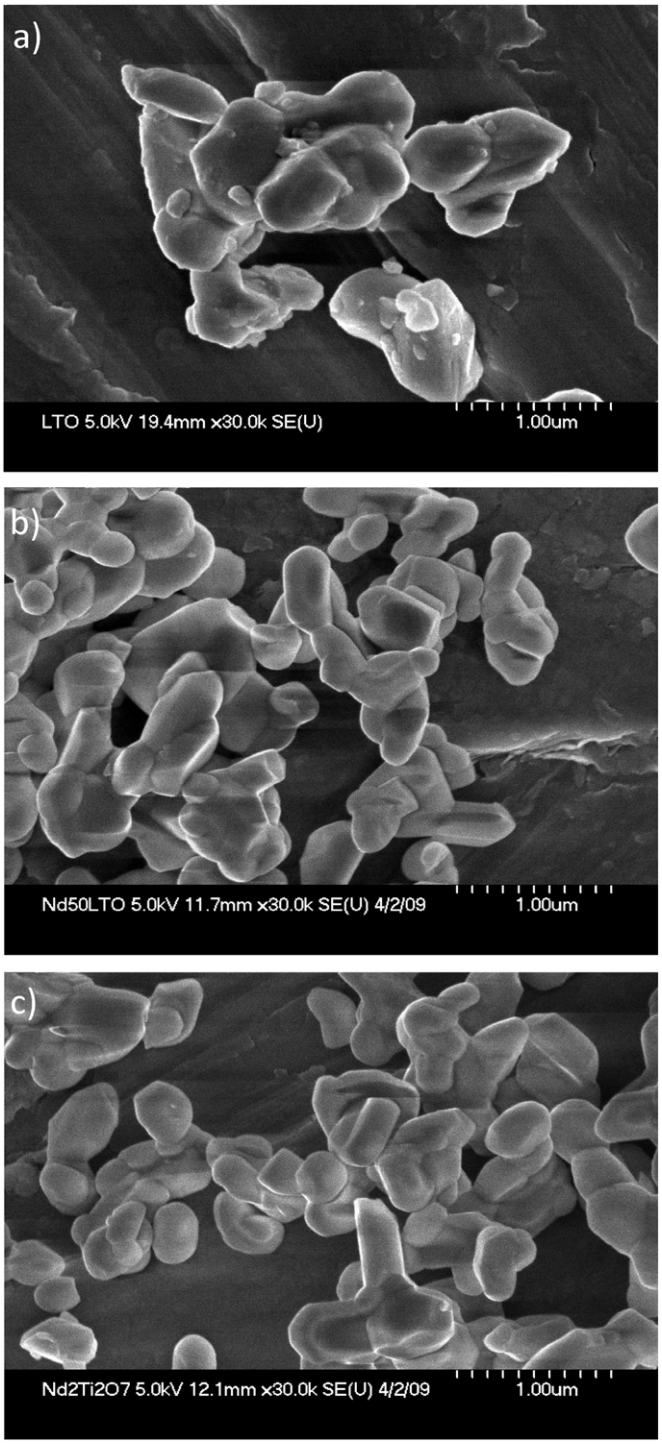

Fig. 7. Typical SEM images of $(La_{1-x}Nd_x)_2Ti_2O_7$ powders for $x=0$, 0.5 and 1: (a) $La_2Ti_2O_7$, (b) $LaNdTi_2O_7$ and (c) $Nd_2Ti_2O_7$.

3.3. Electric properties

3.3.1. Dielectric properties

The ceramics used for the dielectric permittivity and losses measurements were obtained after a preliminary treatment of powders at 1100 °C and then sintering in pellets at 1250 °C under air. In these conditions, the compactness of the pellets was in the range of 86–95% for all the compositions.

Firstly, the frequency dependences of the dielectric characteristics, i.e. real part of permittivity and tangent loss, at room temperature are shown in Fig. 8a and b (low-frequency range: 10^1–10^6 Hz) and Fig. 8c and d (high frequency range: 10^7–10^9 Hz), respectively. The first observation is that the low-frequency values of permittivity are in the range 10–80, the smallest values belonging to the composition $x=0$, while the other compositions have ε_r in the range 50–80. However, the real part of permittivity increases to a maximum of 50 at% ($LaNdTi_2O_7$), and then decreases for higher substitution rates (Fig. 8a). A large range of frequencies (10^1–10^6 Hz), where the permittivity is almost unchanged shows the lack of any dielectric relaxation phenomena. At very low frequencies (10^1–10^2 Hz), although the noise is higher, it is possible

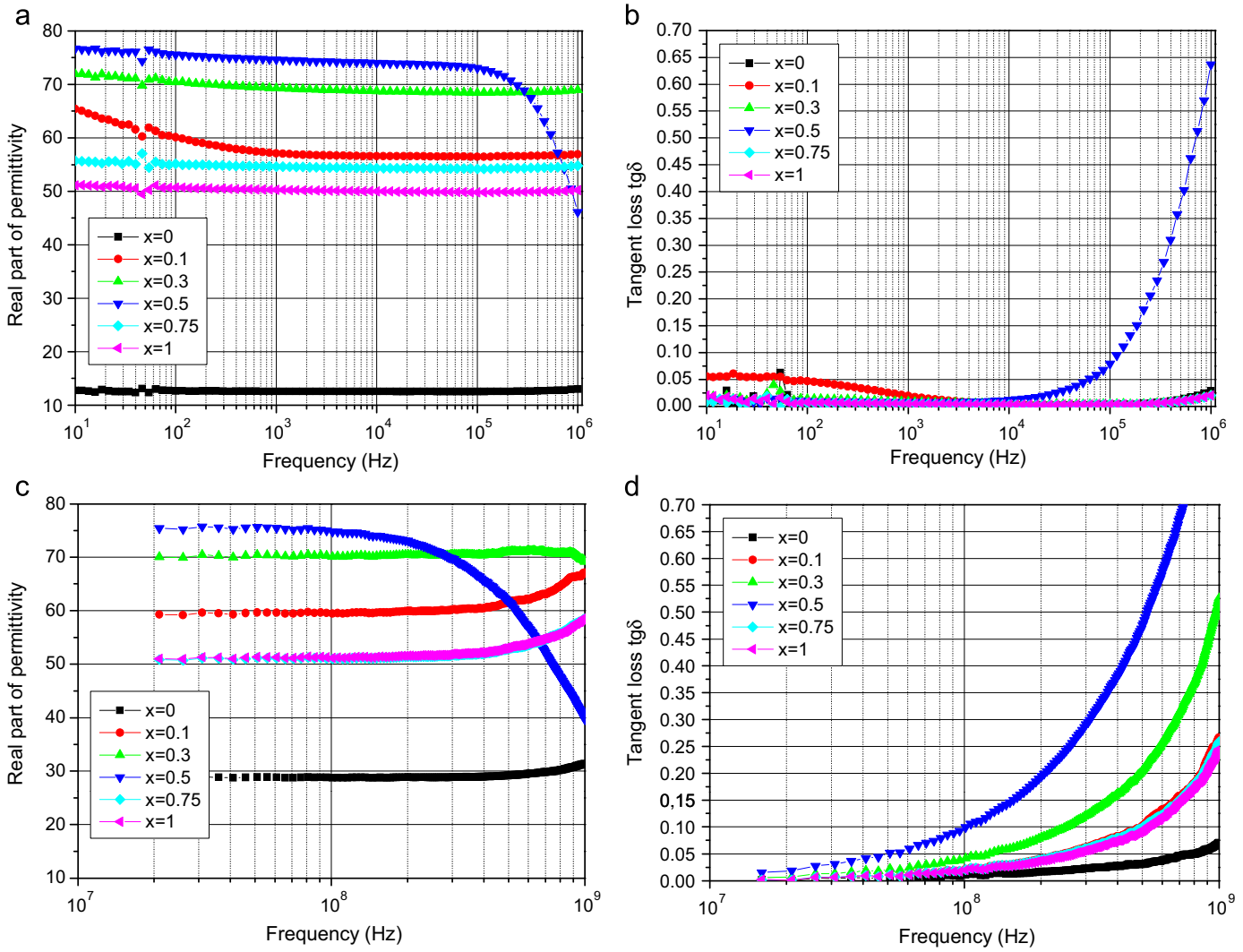

Fig. 8. Frequency dependence of the dielectric properties of the $(La_{1-x}Nd_x)_2Ti_2O_7$ $(0 \le x \le 1)$ ceramics sintered at 1100 °C under air (range 10–10^6 Hz): (a) real part of permittivity, (b) tangent loss (range 10^7–10^9 Hz), (c) real part of permittivity and (d) tangent loss.

to notice the increasing permittivity associated with increasing losses for the composition $x=0.1$, which seems to possess a higher dc-conductivity component or Maxwell–Wagner relaxation, most probably due to some degree of local electrical heterogeneity within the ceramic sample. A particular behavior is shown by the composition $x=0.5$ around 10^6 Hz, which manifests with a strong decrease in the permittivity and increasing losses, which are a sign of a dipolar dielectric relaxation in this frequency range. All the other compositions seem to follow the same tendency, as it can be better noticed in the increasing losses at high frequencies shown in the inset of Fig. 8b. Therefore, all the compositions have above 10^6 Hz a kind of dipolar relaxation which is better evidenced for $x=0.5$. The high frequency range presents interesting dielectric behavior (Fig. 8c). After almost constant permittivity of 20–75 for frequencies ranging from 10^7 to 2×10^8 Hz, all the compositions show an increase around 10^9 Hz accompanied by a strong increase in the tangent loss towards unity (Fig. 8d), indicating that some relaxation processes take place at these frequencies. The only exception is again the composition $x=0.5$, showing a very strong dispersion starting from 10^8 Hz, which manifests with a fast decrease when the frequency increases. A small decrease of permittivity at high frequencies also is shown by the composition $x=0.3$, while the compositions $x=0.1$, 0.75 and 1 show an increase of permittivity when frequency approaches 10^9 Hz. In conclusion of this part, all the compositions $(La_{1-x}Nd_x)_2Ti_2O_7$ $(0 \le x \le 1)$ present at room temperature good dielectric properties, low losses and permittivities of tenths, and dispersion phenomena in the range of frequencies of $\sim10^6$ and $\sim10^9$ Hz, slightly dependent on composition. The origin and type of these dispersions (dipolar relaxation, resonances) cannot be elucidated at this stage, also due to the fact that these phenomena are out of the measurement range and without a study of temperature-variation of the dielectric properties.

In order to have a better insight on the dielectric behavior of the ceramics, samples cooled in O_2 were synthesized to avoid the possible formation of Ti^{3+}. The presence of Ti^{3+} was recently reported by West et al. in $BaTiO_3$ ceramics [37] and by Joseph et al. [6] in $La_2Ti_2O_7$ compounds to induce luminescence properties. To check the presence or absence of Ti^{3+} in our samples cooled in air, spectrofluorimetry experiments were performed (see Section 3.4). In this spirit, the low value of permittivity for $La_2Ti_2O_7$ compared to other compositions cooled in air could be explained by the existence of Ti^{3+} cations, which induce a decrease of the permittivity by conduction phenomenon. Three compositions ($x=0$, 0.5 and 1) were taken into profit in this study knowing that no change in the structural properties was observed on the XRD patterns compared to the pellets cooled down in air. The frequency dependence of the dielectric characteristics, i.e.

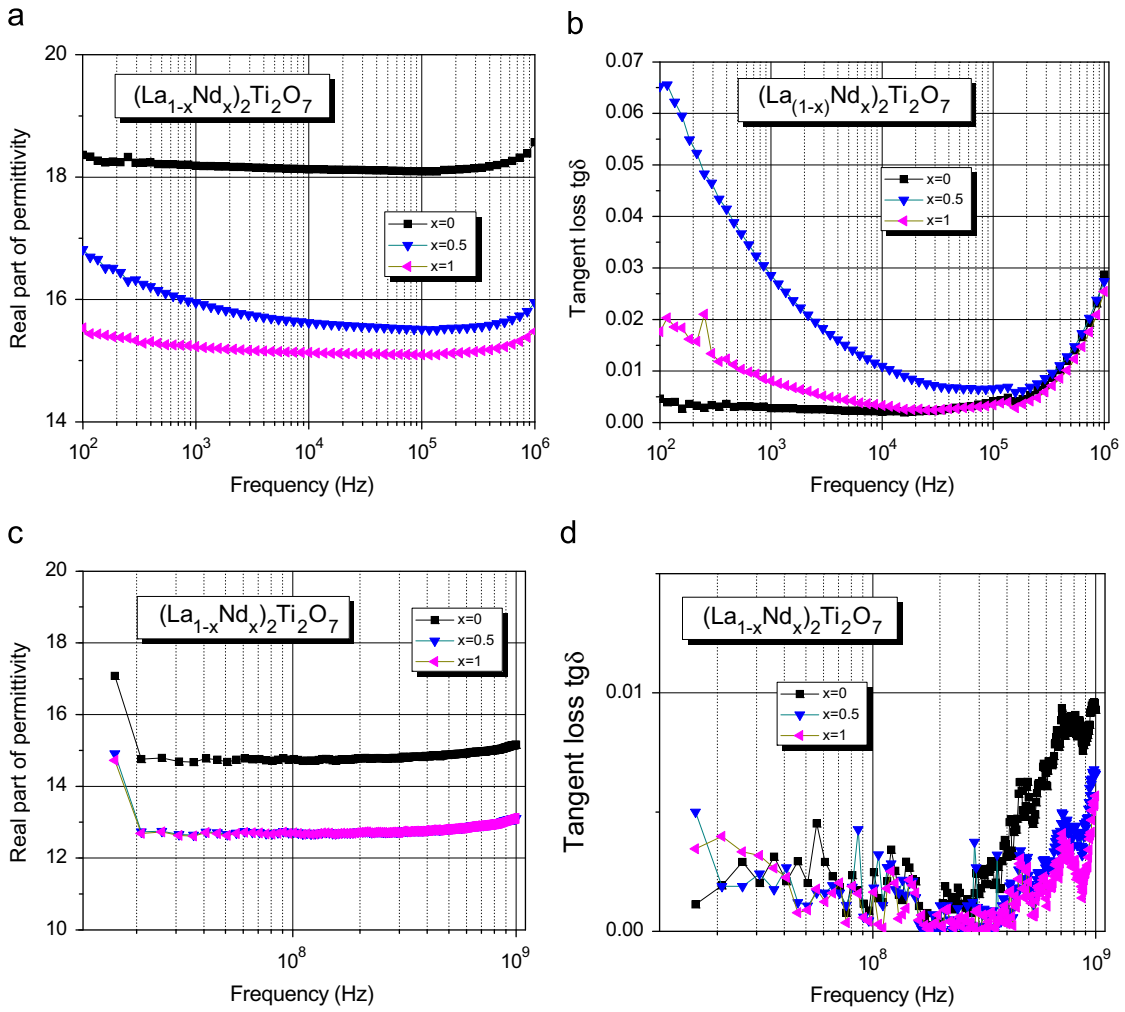

Fig. 9. Frequency dependence of the dielectric properties of the $(La_{1-x}Nd_x)_2Ti_2O_7$ ($x=0$, 0.5 and 1) ceramics sintered at 1100 °C under O_2 (range 10–10^6 Hz): (a) real part of permittivity, (b) tangent loss (range 10^7–10^9 Hz), (c) real part of permittivity and (d) tangent loss.

real part of permittivity and tangent loss, at room temperature is shown in Fig. 9a and b (low-frequency range: 10^2–10^6 Hz) and Fig. 9c and d (high frequency range: 10^7–10^9 Hz), respectively. The recorded permittivity values are in the range of 10–20 in the investigated frequency range. The tangent loss is below 3% for all the compositions at 1 kHz and below 7% in the low-frequency range. Thus, the solid solution shows rather good dielectric characteristics at low frequencies. The frequency dependence of the dielectric constant and tangent loss is very similar for the three compositions in the range of 10^2–10^6 Hz, indicating that similar dielectric relaxations are governing the dielectric characteristics, irrespective of compositions. The large range of frequencies, 10^2–10^6 and 10^7–10^9 Hz, where the permittivity is almost unchanged show the lack of any dielectric relaxation phenomena. Higher losses above 10^6 Hz are related to dipolar relaxation phenomena, which manifest by an increase in the tangent loss (Fig. 9b). The lack of dielectric data in the frequency range 10^6–10^7 Hz does not allow to investigate in detail this relaxation.

The literature presents very scarce data on the dielectric properties of such compounds. Only for the ceramic composition $x=0$, 0.5 and 1, permittivities of ~33–50 were reported at 10^6 Hz [38–40]. These values are comparable to those obtained under air cooling (permittivities of ~12–78). However, the smallest values of permittivity were found for $x=0$, 0.5 and 1 for the ceramics obtained under O_2 cooling (permittivities of ~12–18). This difference of permittivity obtained on ceramics cooled in air or O_2 could be explained by the difficulty of obtaining compact ceramics. Indeed, under O_2, compactness is less important than the pellets made in air (78–85%). Actually, the limitation in terms of obtaining more dense microstructure is related to the appearance of additional peaks on the XRD patterns if performing the sintering at higher temperatures. Although densities above 90% are normally required for the electrical investigations, due to the mentioned limitations related to preserving the phase purity in our compounds, we have not obtained such high densities. So, these various degrees of porosity, in these ceramics, could explain such an evolution. However, for $La_2Ti_2O_7$ and contrary to $Nd_2Ti_2O_7$ or $LaNdTi_2O_7$, the variation of the permittivity is not significant for ceramics cooled in air and O_2. Logically, it should also decrease with the decrease of compactness. This observation could be consistent with the presence of Ti^{3+} cations in LTO. Indeed, in the presence of O_2 during cooling, Ti^{3+} cations are oxidized and their proportion is decreasing. This effect compensates the loss of compactness.

3.3.2. *Qualitative evidence of the piezoelectric properties*

The piezoelectric character was qualitatively demonstrated at high frequencies by using a dielectric holder with two ranges of stress (low/high stress, as allowed by the dielectric holder of the Agilent E4991A RF system). Fig. 10 shows the increasing permittivity values of $(La_{1-x}Nd_x)_2Ti_2O_7$ elaborated in O_2 cooling

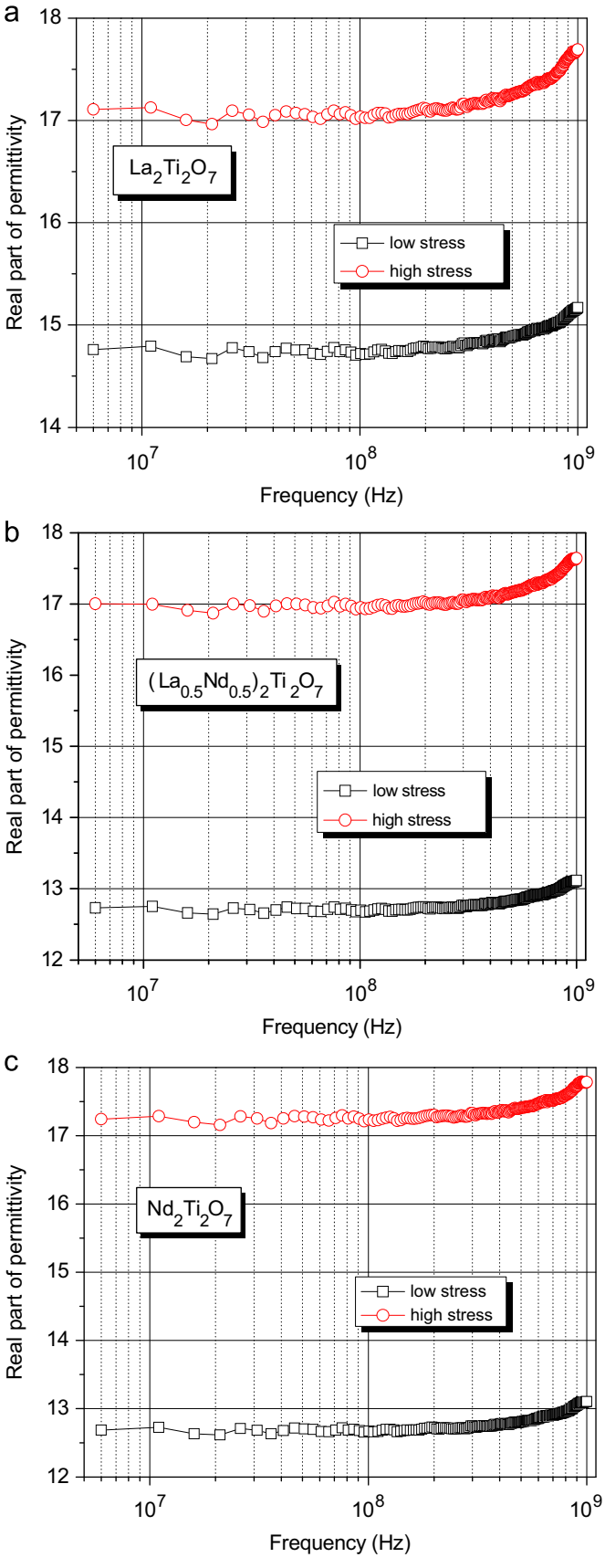

Fig. 10. The stress effect on the frequency dependence of the dielectric constant in $(La_{1-x}Nd_x)_2Ti_2O_7$ ceramics with $x=0$, 0.5 and 1.

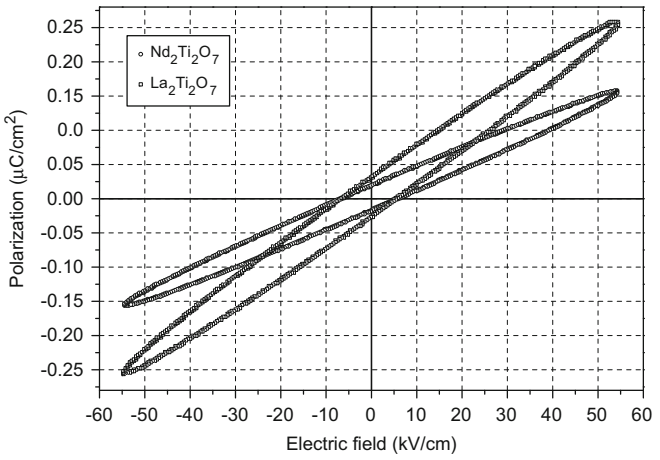

Fig. 11. $P(E)$ loops measured on $(La_{1-x}Nd_x)_2Ti_2O_7$ ceramics with compositions: $x=0$ and 1. $(La_{0.5}Nd_{0.5})_2Ti_2O_7$ intermediate composition shows a trend similar to that obtained for $x=1$.

for the three compositions $x=0$, 0.5 and 1 as a result of the mechanical stress. Relative variations ~15% for $La_2Ti_2O_7$ and ~30% for $LaNdTi_2O_7$ and $Nd_2Ti_2O_7$ for the permittivity clearly demonstrate the piezoelectric character of these compositions and confirm the observations of Ref. [39]. However, the piezoelectric properties of these compounds have to be analyzed in detail in dense ceramics, for which a detailed study would reveal the nature of piezoelectricity and its relationship with microstructural parameters and composition. This objective will be a further study.

3.3.3. Ferroelectric properties

$P(E)$ loops recorded on $La_2Ti_2O_7$, $LaNdTi_2O_7$ and $Nd_2Ti_2O_7$ ceramics allowed to evidence a certain degree of non-linearity and small hysteresis (Fig. 11), which might be a sign of the ferroelectric hysteretic $P(E)$ nonlinear dependence. The $LaNdTi_2O_7$ and $Nd_2Ti_2O_7$ compounds have a similar characteristic hysteresis loop while the $La_2Ti_2O_7$ compound has a higher slope. Measured values (coercive fields, polarization) are in good agreement with previous ones reported in the literature for the bulk $La_2Ti_2O_7$ composition [9]. However, the available fields (<10 kV/mm) did not allow us to reach full saturation of the ceramic samples and to undoubtly decide if a macroscopic ferroelectric character was achieved in the present compounds or if another type of non-linear character (e.g. non-linear losses, resistivity) is responsible for the observed $P(E)$ dependence. Sayir et al. [9] also indicated the difficulty to reach the saturation and attribute that with the low crystal symmetry ($P2_1$) of LTO, and consequently, to the difficulty to polarize randomly oriented polycrystalline ceramics. The dipole moment in $A_{n+1}B_{n+1}O_{3n+5}$ ($A_4B_4O_{14}$ for $n=3$) structure is only generated by the displacement of the interlayer through a cation displacement in the (100) cleavage plane that is parallel to the b-axis (polar axis) [18]. In our case, this difficulty of saturation is enhanced by the low density of our ceramics. However, given the low symmetry of the unit cell (i.e. compatible with a ferroelectric unit cell distortion), the quite high observed permittivity (in the range of tenths), the piezoelectricity and nonlinear $P(E)$ trends, it seems that a ferroelectric character is most probably present. The observed properties might recommend these ceramic compounds as possible candidates for tunability applications. In case of $BaTiO_3$-based ferroelectrics with high permittivity, one way to reduce the permittivity while preserving high nonlinear $\varepsilon(E)$ character is to create composites with a low-permittivity linear dielectric [41]. However, the increasing dielectric losses with frequency in GHz range found

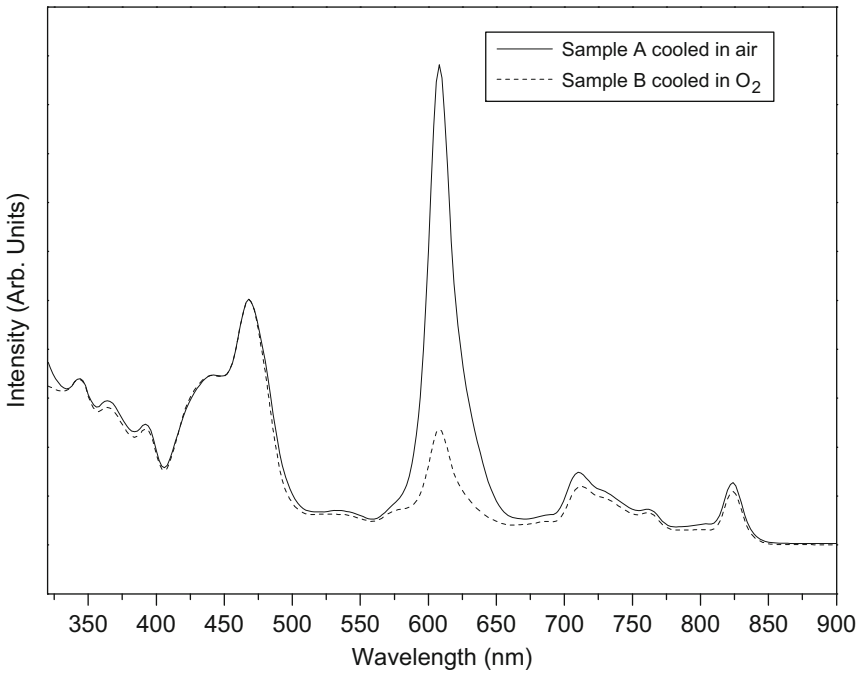

Fig. 12. Emission spectra of $La_2Ti_2O_7$ cooled in static air (sample A) and cooled in O_2 (sample B) under laser excitation at 292 nm.

for these ceramics have to be well understood and further controlled for possible tunability applications. In conclusion, the origin and characteristics of dielectric, piezoelectric and ferroelectric properties of $(La_{1-x}Nd_x)_2Ti_2O_7$ solid solutions are not understood in depth and these ceramics have to be carefully investigated in the future. In order to perform such an investigation, the optimum conditions for sintering have to be firstly determined in order to increase the density above 95%, while preserving the phase purity. Alternative sintering routes as spark plasma sintering might be a valuable alternative for this aim [42].

3.4. Luminescence properties

Joseph et al. [6] indicate that La^{3+} ions without 4*f* electrons have no electronic energy levels that can induce excitation and luminescence processes in the visible region, whereas the presence of the Ti^{3+} ions leads to luminescence in this region. Then, to check the presence of Ti^{3+} in our compounds, and its effect on luminescence properties, two $La_2Ti_2O_7$ pellets sintered in different manners were selected: sample A was obtained after cooling under static air whereas sample B was obtained under pure oxygen. Pellets A and B were then grinded for photoluminescence experiments. The absorption spectra were collected with a SAFAS FLX-Xenius spectrofluorimeter using a laser excitation at 292 nm (xenon source) and allowing the acquisition of emission spectrum in the 320–900 nm range.

If one considers the sharp peak centered at ~610 nm, by comparison between samples A and B, this band appears significantly stronger compared to the former (see Fig. 12). It has been reported in literature [6,43] that the metal activator Ti^{3+} ions have spectral stimulated emission (SE) near 611 nm with the channel $^2E \rightarrow {}^2T_2$. Electronic transitions of the La^{3+} enhance this SE. So, the proportion of Ti^{3+} species should be significantly weakened after oxygen treatment, which is observed in the present case. Note however that the enhancement of dielectric properties for Ti-based perovskites such as $BaTiO_3$, after cooling under oxygen, is well known and has already been reported [37].

4. Conclusion

$(La_{1-x}Nd_x)_2Ti_2O_7$ oxides were successfully synthesized by sol–gel method and studied by X-ray diffraction and scanning electron microscopy. The characterization results showed the formation of a complete solid solution, whatever the *x* value. $(La_{1-x}Nd_x)_2Ti_2O_7$ has a layered perovskite structure built of layers of distorted perovskite-like slabs running parallel to the (110) plane bounded to each other by interlayer La^{3+} and/or Nd^{3+} ions. Whatever the substitution, compounds are isomorphous with monoclinic symmetry ($P2_1$ space group). The SEM analysis shows the homogenous powders in size, shape and the quantitative atomic repartition of elements. The electrical measurements performed on the ceramic series show good dielectric characteristics with low tangent losses below 10^6 Hz. Permittivity of tenths (12–78) was found for all the compositions. Piezoelectricity at room temperature was also qualitatively demonstrated. Unsaturated nonlinear *P*(*E*) hysteresis loops were obtained; they might be originated in true ferroelectricity, but contributions from other nonlinear phenomena are not excluded.

Acknowledgments

The authors gratefully acknowledge the Nord-Pas de Calais Region and the Centre National de la Recherche Scientifique (CNRS) for their financial support linked at this work. Specifically, this study was conducted as part of a MaProSu project. We also thank Nora Djelal for her help with scanning electron microscopy.

References

[1] M. Uno, A. Kosuga, M. Okui, K. Horisaka, S. Yamanaka, J. Alloys Compd. 400 (2005) 270–275.

[2] H. Song., T. Peng, P. Cai., H. Yi, C. Yan, Catal. Lett. 113 (1–2) (2007) 54–58.
[3] S. Otsuka-Yao-Matsuo, T. Omata, M. Yoshimura, J. Alloys Compd. 376 (2004) 262–267.
[4] C.E. Bamberger, H.W. Dunn, G.M. Begun, S.A. Landry, J. Less Common Met. 109 (1985) 209–217.
[5] P.T. Diallo, P. Boutinaud, R. Mahiou, J. Alloys Compd. 341 (2002) 139–143.
[6] L.K. Joseph, K.R. Dayas, S. Damodar, B. Krishnan, K. Krishnankutty, V.P.N. Nampoori, P. Radhakrishnan, Spectrochim. Acta Part A 71 (2008) 1281–1285.
[7] W.S. Kim, S.M. Ha, S. Yun, H.H. Park, Thin Solid Films 420 (2002) 575–578.
[8] W.S. Kim, S.M. Ha, J.K. Yang, H.H. Park, Thin Solid Films 398 (2001) 663–667.
[9] A. Sayir, S.C. Farmer, F. Dynys, Ceram. Trans. 179 (2006) 57–68.
[10] P. Dasgupta, Y.M. Jana, A. Nag Chattopadhyay, R. Higashinaka, Y. Maeno, D. Ghosh, J. Phys. Chem. Solid 68 (2007) 347–354.
[11] A.V. Shlyakhtina, A.V. Knotko, M.V. Boguslavskii, S.Y. Stefanovich, D.V. Peryshkov, I.V. Kolbanev, L.G. Shcherbakova, Solid State Ionics 176 (2005) 2297–2304.
[12] M.A. Subramanian, G. Aravamundan, G.V. Subba Rao, Prog. Solid. State Chem. 15 (1983) 55–143.
[13] R.D. Shannon, Acta Crystallogr. A 32 (1976) 751–767.
[14] S. Nanamatsu, M. Kimura, J. Phys. Soc. Japan 36 (1974) 1495.
[15] S. Nanamatsu, M. Kimura, K. Doi, S. Matsushita, N. Yamada, Ferroelectrics 8 (1974) 511–513.
[16] N. Ishizawa, F. Marumo, S. Iwai, M. Kimura, T. Kawamura, Acta Crystallogr. B 38 (1982) 368–372.
[17] H.W. Schmalle, T. Williams, A. Reller, A. Linden, J.G. Bednorz, Acta Crystallogr. B 49 (1993) 235–244.
[18] M. Kimura, S. Nanamatsu, T. Kawamura, S. Matsushita, Jpn. J. Appl. Phys. 13 (9) (1974) 1473–1474.
[19] H.G. Kim, K.W. Hwang, S.W. Bae, J.H. Jung, J.S. Lee, Catal. Lett. 91 (2003) 193–198.
[20] Z. Li, H. Xue, X. Wang, X. Fu, J. Mol. Catal. Chem. A 260 (2006) 56–61.
[21] Z. Li, G. Chen, X. Tian, Y. Li, Mater. Res. Bull. 43 (2008) 1781–1788.
[22] H.B. Song, T.Y. Peng, P. Cai, H.B. Yi, C.H. Yan, Catal. Lett. 113 (1–2) (2007) 54–58.
[23] Z.T. Zhao, Y.M. Zhang, J. Yang, H. Li, W. Song, X.Q. Zhao, J. Ceram. Soc. Japan 113 (1) (2005) 67–70.
[24] A.V. Prasadarao, U. Selvaraj, S. Komarneni, A.S. Bhalla, J. Mater. Res. 7 (10) (1992) 2859–2863.
[25] D.S. Todorovsky, M.M. Getsova, M.A. Vasileva, J. Mater. Sci. 37 (2002) 4029–4039.
[26] A.M. Sych, Yu.A. Titov, L.F. Nedil'ko, B. Tanirbergenov, K.U. Baimbetov, S.G. Andreeva, Zh. Neorg. Khim. 32 (11) (1987) 2625–2628.
[27] D.W. Hwang, J.S. Lee, W. Li, S.H. Oh, J. Phys. Chem. B 107 (2003) 4963–4970.
[28] Y. Shimada, H. Kiyama, Y. Tokura, Phys. Rev. B: Condens. Matter Mater. Phys. 75 (2007) 245125.
[29] N.A. Zakharov, E.F. Kustov, V.S. Krikorov, S.Y. Stefanovich, V.B. Loshchenov, Pis'ma Zh. Tekh. Fiz. 4 (17) (1978) 1043–1046.
[30] J. Takahashi, K. Kageyama, K. Kodaira, Jpn. J. Appl. Phys. 32 (1993) 4327–4331.
[31] J. Takahashi, K. Kageyama, T. Hayashi, Jpn. J. Appl. Phys. 30 (9B) (1991) 2354–2358.
[32] Z. Shao, S. Saitzek, P. Roussel, M. Huvé, R. Desfeux, O. Mentré, F. Abraham, J. Cryst. Growth 311 (16) (2009) 4134–4141.
[33] T.J.B. Holland, S.A.T. Redfern, J. Appl. Crystallogr. 30 (1997) 84–85.
[34] L. Vegard, Z. Phys. 5 (1921) 17–26.
[35] V.V. Atuchin, T.A. Gavrilova, J.-C. Grivel, V.G. Kesler, Surf. Sci. 602 (19) (2008) 3095–3099.
[36] V.V. Atuchin, T.A. Gavrilova, J.-C. Grivel, V.G. Kesler, J. Phys. D: Appl. Phys. 42 (2009) 035305.
[37] N. Masó, H. Beltran, E. Cordoncillo, D.E. Sinclair, A.R. West, J. Am. Ceram. Soc. 91 (1) (2008) 144–150.
[38] Y.J. Zhong, F. Azough, R. Freer, J. Eur. Ceram. Soc. 15 (3) (1995) 255–263.
[39] J.K. Yamamoto, A.S. Bhalla, J. Appl. Phys. 70 (1991) 4469–4471.
[40] J. Takahashi, K. Kageyama, T. Hayashi, Jpn. J. Appl. Phys. 30 (9B) (1991) 2354–2358.
[41] A.K. Tagantsev, V.O. Sherman, K.F. Astafiev, J. Venkatesh, N. Setter, J. Electroceram. 11 (2003) 5–66.
[42] Z. Shen, Z. Zhao, H. Peng, M. Nygren, Nature 417 (2002) 266–269.
[43] A.A. Kaminskii, in: Crystalline Lasers: Physical Processes and Operating Schemes, CRC Press, USA, 1996 (Chapter 1).